THE JOURNAL OF PHYSICAL CHEMISTRY Letters

Letter

pubs.acs.org/JPCL

Size-Dependent Photon Emission from Organometal Halide Perovskite Nanocrystals Embedded in an Organic Matrix

Dawei Di,*[,†] Kevin P. Musselman,[†] Guangru Li,[†] Aditya Sadhanala,[†] Yulia Ievskaya,[‡] Qilei Song,[†,§] Zhi-Kuang Tan,[†] May Ling Lai,[†] Judith L. MacManus-Driscoll,[‡] Neil C. Greenham,[†] and Richard H. Friend*[,†]

[†]Cavendish Laboratory, University of Cambridge, JJ Thomson Avenue, Cambridge CB3 0HE, United Kingdom

[‡]Department of Materials Science and Metallurgy, University of Cambridge, 27 Charles Babbage Road, Cambridge CB3 0FS, United Kingdom

[§]Department of Chemical Engineering, Imperial College London, London SW7 2AZ, United Kingdom

Supporting Information

ABSTRACT: In recent years, organometal halide perovskite materials have attracted significant research interest in the field of optoelectronics. Here, we introduce a simple and low-temperature route for the formation of self-assembled perovskite nanocrystals in a solid organic matrix. We demonstrate that the size and photoluminescence peak of the perovskite nanocrystals can be tuned by varying the concentration of perovskite in the matrix material. The physical origin of the blue shift of the perovskite nanocrystals' emission compared to its bulk phase is also discussed.

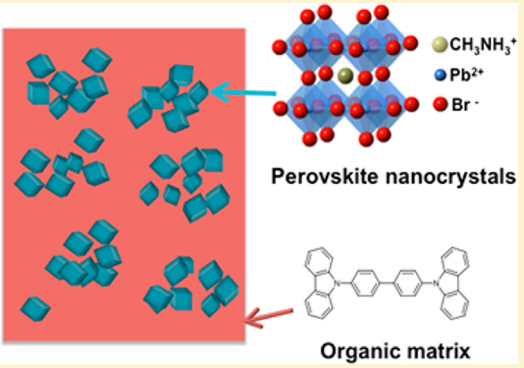

Organometal halide perovskites (Pe's) have emerged as a promising class of materials for photovoltaic applications.[1−5] Recently, we demonstrated the first organometal halide Pe light-emitting diodes (PeLEDs),[6] based on $CH_3NH_3Pb(I_{1-x}Br_x)_3$, tunable in emission color from the near-infrared (x = 0) to green (x = 1). The material also exhibits efficient lasing under optical pumping.[7,8] These findings indicate that Pe-based devices, which can be solution-processed, are promising alternatives to organic light-emitting diodes (OLEDs), in addition to their application as a solar energy harvester.

The majority of investigations to date concern the bulk properties of the Pe, despite the fact that the formation of nanometer-sized structures was noted in the pioneering work by Kojima et al.[1] Recently, Schmidt et al. reported a synthetic chemistry route to produce 6 nm sized organometal Pe colloidal nanoparticles.[9] Engineered nanostructures, including nanocrystals of many representative inorganic semiconductors such as CdSe,[10,11] InP,[12,13] and Si,[14−17] have shown interesting size-dependent optical and electronic properties that differ significantly from their bulk counterparts. So far, however, there is no literature available concerning the ability to tune the size of the Pe nanocrystals and their size-dependent properties.

In this Letter, we introduce a simple, low-temperature approach for the formation of self-assembled Pe nanocrystals in a solid organic matrix. As organometal halide Pe's crystallize rapidly even at room temperature, we expect that it is possible to form Pe nanocrystals in a solid matrix at temperatures below 100 °C. We demonstrate that the size and photoluminescence (PL) peak of the Pe nanocrystals produced at <100 °C can be tuned by varying the concentration of Pe in the matrix material. Finally, we discuss the physical origin of the PL blue shift of the Pe nanocrystals that we observe compared to the bulk phase.

A $CH_3NH_3PbBr_3$ Pe precursor solution (CH_3NH_3Br and $PbBr_2$ dissolved in *N*,*N*-dimethylformamide (DMF)) and a 4,4-bis(*N*-carbazolyl)-1,1-biphenyl (CBP) matrix solution were prepared and mixed to achieve various weight ratios between the CBP and the Pe precursor (CBP/Pe = 1:1, 3:1, 4:1, 10:1 and 15:1). The mixtures were stirred at 70 °C for 2 h and were spun-cast onto precleaned quartz substrates in a N_2 glovebox to obtain a film thickness of ∼50 nm. CBP (HOMO = −6.0 eV; LUMO = −2.9 eV) is a high-performance host material widely used in phosphorescent OLEDs.[18] The thin films were then annealed at 90 °C for 5 min to accelerate solvent evaporation and crystallization. The crystal structure of $CH_3NH_3PbBr_3$ Pe, the molecular structure of CBP, and the general processing sequence for obtaining Pe nanocrystals in an organic matrix are outlined in Figure 1. To observe whether Pe nanocrystal formation also occurs in other types of organic matrixes such as polymer materials, polystyrene (PS) was dissolved in DMF at a

Received: December 11, 2014
Accepted: January 14, 2015
Published: January 14, 2015

DOI: 10.1021/jz502615e
J. Phys. Chem. Lett. 2015, 6, 446−450

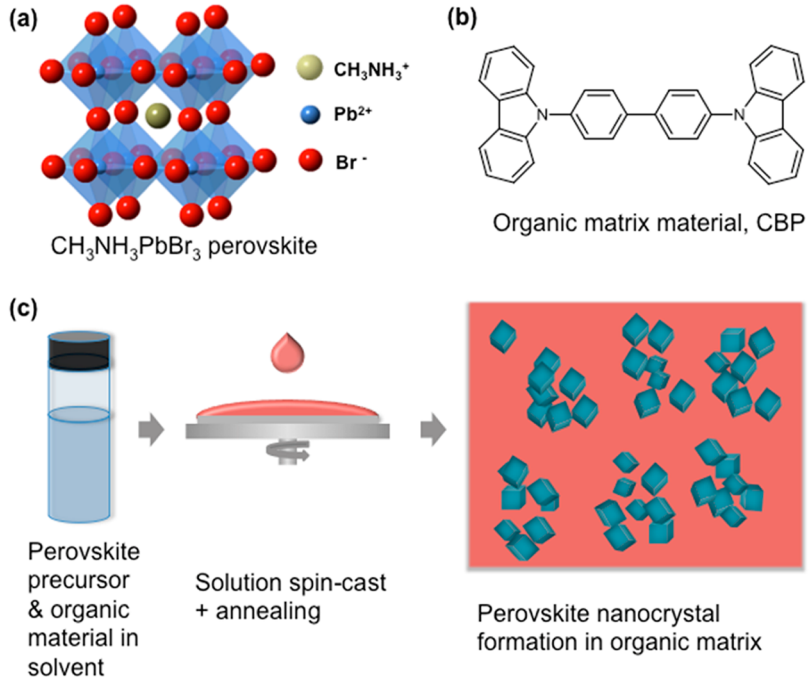

Figure 1. Schematic diagrams of materials and processes. (a) Crystal structure of $CH_3NH_3PbBr_3$. (b) Molecular structure of CBP. (c) Fabrication sequence of Pe nanocrystals in an organic matrix.

concentration of 20 mg/mL and mixed with the Pe precursor solution at a 10:1 ratio, followed by the same spin-cast and annealing processes, to obtain a PS/Pe nanocrystal thin film.

To investigate the morphology and distribution of Pe nanocrystals formed in organic matrixes, we studied the films using scanning electron microscopy (SEM). Figure 2 shows plan-view SEM images of the CBP/Pe samples mixed at different weight ratios (1:1, 3:1, and 15:1). Images of samples with ratios of 4:1 and 10:1 are available in the Supporting Information. The brighter regions in the micrographs correspond to $CH_3NH_3PbBr_3$ Pe, while the darker regions correspond to the CBP matrix. The contrast between the two materials is due to the difference in their electron densities. When the weight concentration of Pe is 50% (CBP/Pe =1:1; Figure 2a), the Pe material forms a connected network, decorated by isolated islands of CBP. The mean width of the Pe clusters is ∼280 nm. It appears that the Pe domains are formed by many much smaller nanocrystals. However, it is difficult to resolve the sizes of these small nanocrystals from the SEM images. It is highly likely that phase separation between the Pe nanocrystals and the organic matrix occurred at the same time as Pe crystallization. Also, it can be seen that as the concentration of Pe decreases, the Pe materials form isolated domains with smaller sizes. In the sample with the least amount of Pe material embedded within (CBP/Pe = 15:1; Figure 2c), the average domain size is ∼50 nm. Similarly, we found that it is possible to form Pe nanocrystal domains in a polymer material such as PS (Supporting Information). Figure S1c (Supporting Information) shows the presence of Pe domains (∼180 nm) in a PS matrix at a PS/Pe weight ratio of 10:1. High-resolution SEM images of Pe nanocrystals within the PS matrix were more difficult to obtain due to the insulating nature of the PS matrix.

In order to determine the average sizes of the Pe nanocrystals, the CBP/Pe thin films were examined using X-ray diffraction (XRD). The results are shown in Figure 3a. Two distinct diffraction peaks were found at 14.95° and 30.15°, which correspond to (100) and (200) $CH_3NH_3PbBr_3$ crystalline peaks (cubic structure with lattice parameter of 5.9 Å), respectively. These are in good agreement with the $CH_3NH_3PbBr_3$ XRD peak positions reported by Kojima et al.[1] The intensities of the XRD peaks were mainly limited by the sample thickness (∼50 nm), which was constrained by the low solubility of the organic material in the solvent. Outside of the 2θ range shown in the plot, there were no peaks observable. The very broad peak centered at around 21.5° originates from the quartz substrate. (The reasons for using quartz substrates for XRD analysis were (i) the materials do not adhere very well onto crystalline substrates such as Si and (ii) it ensures the self-consistency of our experiments as the film formation and nanocrystal growth mechanisms may vary for different substrates. Quartz substrates were the most suitable choice as they were also used for the optical measurements discussed later.) As the concentration of Pe in the matrix decreased, a reduction of peak intensity accompanied by peak broadening was observed for the two Pe peaks, indicating a reduction in the size of the nanocrystallites. The average sizes of the Pe nanocrystals were estimated from the more prominent (100) peaks using the Scherrer equation.[19] The average nanocrystal sizes calculated from the XRD results are ∼76, ∼52, ∼24, ∼15, and ∼10 nm for samples with CBP/Pe weight ratios of 1:1, 3:1, 4:1, 10:1, and 15:1, respectively. Therefore, the actual grain sizes are considerably smaller than the sizes of the Pe domains observed in the SEM images, suggesting that each Pe domain contains many smaller nanocrystals.

To examine whether the nanoscale dimension of the Pe material has an impact on its optical properties, we measured the PL spectra of the samples. The PL spectra of samples with Pe nanocrystals embedded in the CBP matrix are shown in Figure 3b. The PL peak position exhibits a monotonic shift toward shorter wavelength as the Pe concentration in the CBP matrix becomes smaller and the average size of the Pe nanocrystals decreases (as evidenced in the XRD measure-

DOI: 10.1021/jz502615e
J. Phys. Chem. Lett. 2015, 6, 446−450

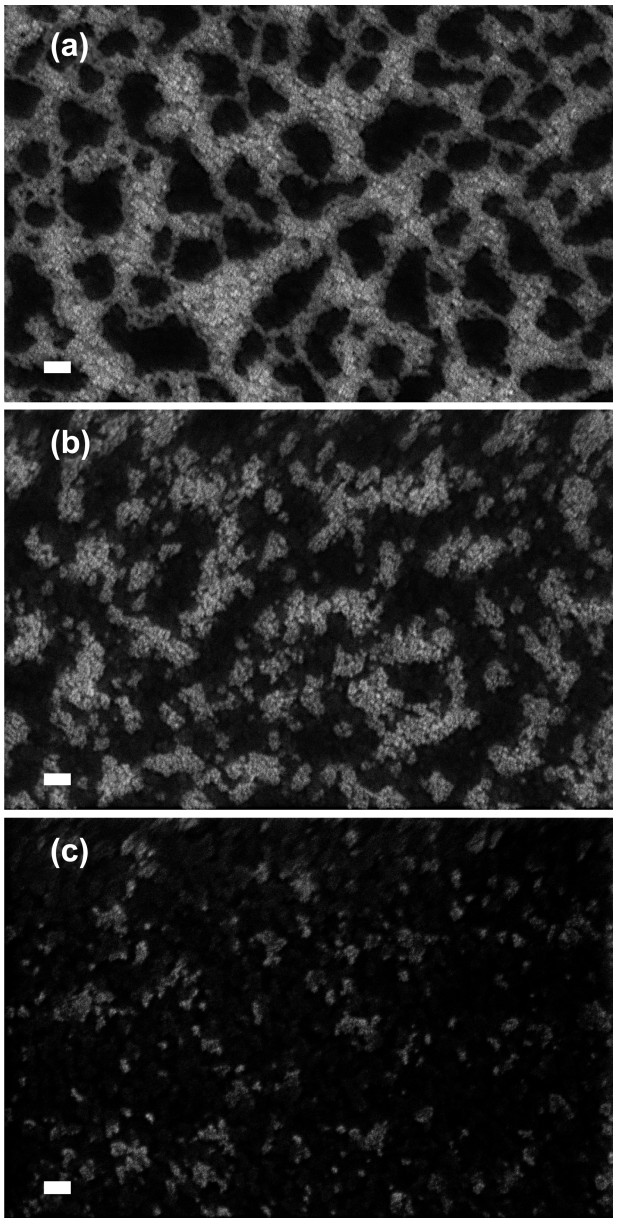

Figure 2. SEM images of $CH_3NH_3PbBr_3$ Pe domains in CBP matrixes with a variation in CBP/Pe weight ratios. The relatively bright regions in the micrographs correspond to domains of $CH_3NH_3PbBr_3$ Pe, while the darker regions correspond to the CBP matrix. Scale bar: 200 nm. CBP/Pe = (a) 1:1, (b) 3:1, and (c) 15:1.

ments). Our results suggest that it is possible to produce size- and color-tunable Pe nanocrystals in an organic matrix by simple solution processing and low-temperature annealing. The PL data of a sample with PS matrix are available as Figure S2 in the Supporting Information, showing a blue-shifted PL peak in comparison to the pristine Pe sample. This shows that the blue shift of the PL emission is not specific to the samples with a CBP matrix. Therefore, it is unlikely that the blue shift is caused by a chemical reaction between the Pe and the organic matrix.

In classical semiconductor nanocrystals such as CdSe, the shift in PL emission is usually explained by the quantum confinement effect,[20] which uses the "particle in a box" analogy to describe the increase in the band gap of nanometer-scale structures. The band gap of a quantum-confined structure can be expressed by the equation[20]

$$E_g = E_{g,bulk} + \Delta E_{confinement}$$

where E_g is the effective band gap of the confined system, $E_{g,bulk}$ is the band gap of the bulk material, and $\Delta E_{confinement}$ is the band gap increase due to quantum confinement, which for a cubic box takes the form of $3\hbar^2\pi/2m^*d^2$, where $\hbar$ is the reduced Planck constant, m^* is the effective mass of carriers (reduced mass for electrons and holes), and d is the size of the nanocrystals. As shown in Figure 3c, we found that the optical band gap, as determined from the PL spectra, can be fitted by $E_{PL} = 2.39 + 12/d^2$ eV, where d is the particle size in nm. This suggests that the PL blue shift is a manifestation of quantum confinement of excitons in the Pe nanocrystals. From the fitted equation, we extract an effective carrier mass of ~0.08 m_0, where m_0 is the mass of a free electron. This value is in agreement with the theoretical reduced mass values reported by Umari et al.[21] The small effective mass is responsible for the quantum confinement effect observed at relatively large grain sizes (d > 10 nm), in comparison with II–VI nanocrystals.

To further confirm that the Pe nanocrystal materials prepared in this work have band gap energies higher than the bulk phase, we measured their absorbance spectra by photothermal deflection spectroscopy (PDS)[22] (Figure 3d), a method that can measure accurate absorption data without the influences of optical scattering and interference in thin-film samples. As the concentration of Pe in the organic matrix decreases, a shift of the absorption edge (the shoulder of each absorbance curve) toward higher energies was observed, indicating a positive change in the material's band gap. We found that the PL emission peak of each sample occurs approximately at the same position as its absorption edge. Therefore, the PDS results are in good agreement with the observed blue shift of the PL. This strengthens our view that size-dependent optical band gaps have been achieved in these samples.

In summary, we have demonstrated a simple and low-temperature route to producing self-assembled organometal halide Pe nanocrystals embedded in an organic matrix. We showed that by varying the concentration of the Pe in the matrix, it is possible to control the average size of the Pe nanocrsytals and thereby fine-tune the absorption and emission of the material. Although we demonstrated the concept by focusing on $CH_3NH_3PbBr_3$ nanocrystals in a CBP matrix, our method can be extended to the formation of organometal halide Pe nanocrystals in a wide range of solution-processable materials, including small molecules and polymers that can be dissolved in a common solvent with the Pe material. Our findings could open doors to novel optoelectronic applications that take advantage of the tunability and processing simplicity of the self-assembled Pe nanocrystals. Besides, as the first study of Pe–organic blends, this work may trigger interest in the realization of Pe–organic bulk heterojunction photovoltaics or LEDs. Future work will be centered around the following three aspects: (1) improving the size and distribution uniformity of the organometal halide Pe nanocrystals to achieve narrower emission profiles; (2) further extending the range of the emission spectrum shift and to observe stronger confinement effects by producing smaller Pe nanocrystals; (3) optimizing the processing conditions (e.g., by using alternative matrix materials, processing temperatures, solvents, etc.) toward the fabrication of wavelength-tunable LEDs based on size-tunable, self-assembled Pe nanocrystals.

DOI: 10.1021/jz502615e
J. Phys. Chem. Lett. 2015, 6, 446–450

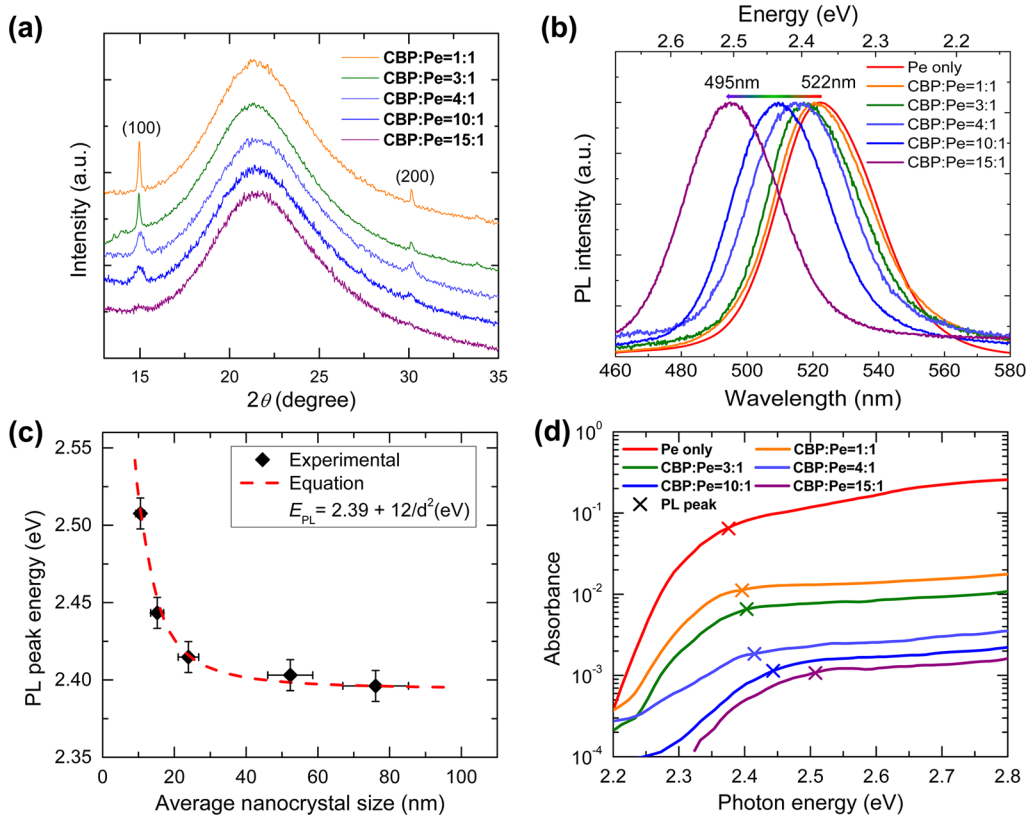

Figure 3. (a) XRD patterns of CBP/$CH_3NH_3PbBr_3$ Pe thin films with various CBP/Pe weight ratios. (b) PL spectra of CBP/Pe samples. The PL spectrum of a bulk (pristine) Pe thin film is also shown (red curve). The peak of the emission shifts to a shorter wavelength as the concentration (and particle size) of Pe in the CBP matrix decreases. The optical excitation was provided by a 407 nm laser. (c) The energy of the PL emission peak as a function of the average Pe nanocrystal size (diamonds). The data can be fitted by $E_{PL} = 2.39 + 12/d^2$ (eV) (dashed line), where d is the particle size in nm. (d) Absorbance data of CBP/Pe samples measured by PDS. Absorbance of a bulk (pristine) Pe thin film is also shown (red curve). The edge (shoulder) of the absorbance band shifts to higher energies as the concentration (and particle size) of Pe in the CBP matrix decreases. The crosses mark the positions of the PL peaks, which roughly coincide with the absorption edges.

EXPERIMENTAL METHODS

Preparation of $CH_3NH_3PbBr_3$ Pe Precursor Solution. $CH_3NH_3PbBr_3$ Pe precursor solution was prepared by mixing CH_3NH_3Br and $PbBr_2$ at a molar ratio of 3:1 in anhydrous DMF (Sigma-Aldrich) to give a weight concentration of 20%. The solution was further diluted in DMF to give a concentration of 10 mg/mL. The solution was stirred for 24 h before further processing.

Preparation of the Solutions of the Organic Matrix Materials. CBP (Sigma-Aldrich) was dissolved in DMF to a concentration of 10 mg/mL. PS (Sigma-Aldrich) was dissolved in DMF to a concentration of 20 mg/mL. The solutions were stirred for 24 h at 70 °C before further processing.

XRD Experiment. The crystallinity of the films was characterized by powder XRD with the help of a Bruker D8 diffractometer with Cu Kα radiation (λ = 1.5418 Å). θ–2θ scans were obtained in the locked coupled mode, sweeping 2θ from 13 to 35° with a 0.02° step size.

SEM. The morphology of the films was examined using a LEO VP1530 field emission SEM.

PL Measurement. The samples were excited by a pulsed laser with 407 nm emission. The Si detector used for capturing the PL spectra was maintained at a temperature of −70 °C.

PDS. Details of the PDS measurement can be found elsewhere.[22]

ASSOCIATED CONTENT

Supporting Information

Additional SEM images of $CH_3NH_3PbBr_3$ perovskite domains in organic molecule and polymer matrixes. PL data of a sample with a PS matrix. This material is available free of charge via the Internet at http://pubs.acs.org.

AUTHOR INFORMATION

Corresponding Authors

*E-mail: rhf10@cam.ac.uk (R.H.F.).
*E-mail: dd403@cam.ac.uk (D.D.).

Notes

The authors declare no competing financial interest.

ACKNOWLEDGMENTS

We thank members of the OE group at the Cavendish Laboratory and members of the Department of Materials Science and Metallurgy for helpful discussions. D.D. acknowledges the Department of Physics, University of Cambridge and the KACST–Cambridge University Joint Centre of Excellence for financial support. G.L. thanks the Gates Cambridge Trust for support. Q.S. acknowledges the Imperial College Junior Research Fellowship. J.L.M.-D. acknowledges ERC Advanced Investigator Grant, Novox, ERC-2009-adG247276. This work was supported by the Engineering and Physical Sciences Research Council, U.K.

DOI: 10.1021/jz502615e
J. Phys. Chem. Lett. 2015, 6, 446–450

REFERENCES

(1) Kojima, A.; Teshima, K.; Shirai, Y.; Miyasaka, T. Organometal Halide Perovskites as Visible-Light Sensitizers for Photovoltaic Cells. *J. Am. Chem. Soc.* **2009**, *131*, 6050−6051.

(2) Lee, M. M.; Teuscher, J.; Miyasaka, T.; Murakami, T. N.; Snaith, H. J. Efficient Hybrid Solar Cells Based on Meso-superstructured Organometal Halide Perovskites. *Science* **2012**, *338*, 643−647.

(3) Burschka, J.; Pellet, N.; Moon, S.-J.; Humphry-Baker, R.; Gao, P.; Nazeeruddin, M. K.; Grätzel, M. Sequential Deposition as a Route to High-Performance Perovskite-Sensitized Solar cells. *Nature* **2013**, *499*, 316−319.

(4) Liu, M.; Johnston, M. B.; Snaith, H. J. Efficient Planar Heterojunction Perovskite Solar Cells by Vapour Deposition. *Nature* **2013**, *501*, 395−398.

(5) Green, M. A.; Ho-Baillie, A.; Snaith, H. J. The Emergence of Perovskite Solar Cells. *Nat. Photonics* **2014**, *8*, 506−514.

(6) Tan, Z.-K.; Moghaddam, R. S.; Lai, M. L.; Docampo, P.; Higler, R.; Deschler, F.; Price, M.; Sadhanala, A.; Pazos, L. M.; Credgington, D.; et al. Bright Light-Emitting Diodes Based on Organometal Halide Perovskite. *Nat. Nanotechnol.* **2014**, *9*, 687−692.

(7) Xing, G.; Mathews, N.; Lim, S. S.; Yantara, N.; Liu, X.; Sabba, D.; Grätzel, M.; Mhaisalkar, S.; Sum, T. C. Low-Temperature Solution-Processed Wavelength-Tunable Perovskites for Lasing. *Nat. Mater.* **2014**, *13*, 476−480.

(8) Deschler, F.; Price, M.; Pathak, S.; Klintberg, L. E.; Jarausch, D.-D.; Higler, R.; Hüttner, S.; Leijtens, T.; Stranks, S. D.; Snaith, H. J.; et al. High Photoluminescence Efficiency and Optically Pumped Lasing in Solution-Processed Mixed Halide Perovskite Semiconductors. *J. Phys. Chem. Lett.* **2014**, *5*, 1421−1426.

(9) Schmidt, L. C.; Pertegás, A.; González-Carrero, S.; Malinkiewicz, O.; Agouram, S.; Espallargas, G. M.; Bolink, H. J.; Galian, R. E.; Pérez-Prieto, J. Nontemplate Synthesis of $CH_3NH_3PbBr_3$ Perovskite Nanoparticles. *J. Am. Chem. Soc.* **2014**, *36*, 850−853.

(10) Peng, X.; Manna, L.; Yang, W.; Wickham, J.; Scher, E.; Kadavanich, A.; Alivisatos, A. P. Shape Control of CdSe Nanocrystals. *Nature* **2000**, *404*, 59−61.

(11) Yen, B. K. H.; Stott, N. E.; Jensen, K. F.; Bawendi, M. G. A Continuous-Flow Microcapillary Reactor for the Preparation of a Size Series of CdSe Nanocrystals. *Adv. Mater.* **2003**, *15*, 1858−1862.

(12) Xie, R.; Battaglia, D.; Peng, X. Colloidal InP Nanocrystals as Efficient Emitters Covering Blue to Near-Infrared. *J. Am. Chem. Soc.* **2007**, *129*, 15432−15433.

(13) Yang, X.; Zhao, D.; Leck, K. S.; Tan, S. T.; Tang, Y. X.; Zhao, J.; Demir, H. V.; Sun, X. W. Full Visible Range Covering InP/ZnS Nanocrystals with High Photometric Performance and Their Application to White Quantum Dot Light-Emitting Diodes. *Adv. Mater.* **2012**, *24*, 4180−4185.

(14) Pavesi, L.; Dal Negro, L.; Mazzoleni, C.; Franzò, G.; Priolo, F. Optical Gain in Silicon Nanocrystals. *Nature* **2000**, *408*, 440−444.

(15) Heitmann, J.; Müller, F.; Zacharias, M.; Gösele, U. Silicon Nanocrystals: Size Matters. *Adv. Mater.* **2005**, *17*, 795−803.

(16) de Boer, W. D. A. M.; Timmerman, D.; Dohnalová, K.; Yassievich, I. N.; Zhang, H.; Buma, W. J.; Gregorkiewicz, T. Red Spectral Shift and Enhanced Quantum Efficiency in Phonon-Free Photoluminescence from Silicon Nanocrystals. *Nat. Nanotechnol.* **2010**, *5*, 878−884.

(17) Conibeer, G.; Green, M. A.; König, D.; Perez-Wurfl, I.; Huang, S.; Hao, X.; Di, D.; Shi, L.; Shrestha, S.; Puthen-Veetil, B.; et al. Silicon Quantum Dot Based Solar Cells: Addressing the Issues of Doping, Voltage and Current Transport. *Prog. Photovoltaics* **2011**, *19*, 813−824.

(18) Gao, Z. Q.; Mi, B. X.; Tam, H. L.; Cheah, K. W.; Chen, C. H.; Wong, M. S.; Lee, S. T.; Lee, C. S. High Efficiency and Small Roll-off Electrophosphorescence from a New Iridium Complex with Well-Matched Energy Levels. *Adv. Mater.* **2008**, *20*, 774−778.

(19) Patterson, A. L. The Diffraction of X-rays by Small Crystalline Particles. *Phys. Rev.* **1939**, *56*, 972.

(20) Brus, L. Electronic Wave Functions in Semiconductor Clusters: Experiment and Theory. *J. Phys. Chem.* **1986**, *90*, 2555−2560.

(21) Umari, P.; Mosconi, E.; Angelis, F. D. Relativistic GW Calculations on $CH_3NH_3PbI_3$ and $CH_3NH_3SnI_3$ Perovskites for Solar Cell Applications. *Sci. Rep.* **2014**, *4*, 4467.

(22) Sadhanala, A.; Deschler, F.; Thomas, T. H.; Dutton, S. E.; Goedel, K. C.; Hanusch, F. C.; Lai, M. L.; Steiner, U.; Bein, T.; Docampo, P.; et al. Preparation of Single-Phase Films of $CH_3NH_3Pb(I_{1-x}Br_x)_3$ with Sharp Optical Band Edges. *J. Phys. Chem. Lett.* **2014**, *5*, 2501−2505.

DOI: 10.1021/jz502615e
J. Phys. Chem. Lett. 2015, 6, 446−450